



**HAL**  
open science

# Rare Palaeomagnetic Evidence of Long-term Mantle Control of the Geodynamo and Possible Role of the NAD-field in the Reversal Process

Kenneth A Hoffman, Pierre Camps, Matt Carlton

► **To cite this version:**

Kenneth A Hoffman, Pierre Camps, Matt Carlton. Rare Palaeomagnetic Evidence of Long-term Mantle Control of the Geodynamo and Possible Role of the NAD-field in the Reversal Process. *Geophysical Journal International*, In press, 10.1093/gji/ggz480 . hal-02367297v1

**HAL Id: hal-02367297**

**<https://hal.science/hal-02367297v1>**

Submitted on 17 Nov 2019 (v1), last revised 21 Oct 2020 (v2)

**HAL** is a multi-disciplinary open access archive for the deposit and dissemination of scientific research documents, whether they are published or not. The documents may come from teaching and research institutions in France or abroad, or from public or private research centers.

L'archive ouverte pluridisciplinaire **HAL**, est destinée au dépôt et à la diffusion de documents scientifiques de niveau recherche, publiés ou non, émanant des établissements d'enseignement et de recherche français ou étrangers, des laboratoires publics ou privés.

# Rare Paleomagnetic Evidence of Long-term Mantle Control of the Geodynamo and Possible Role of the NAD-field in the Reversal Process

Kenneth A Hoffman<sup>1,2</sup>, Pierre Camps<sup>3</sup> & Matt Carlton<sup>1</sup>

1. Physics Department, Cal Poly State University, San Luis Obispo, CA 93407 USA  
khoffman@calpoly.edu
2. Department of Geoscience, University of Wisconsin-Madison, Madison, WI 53706 USA
3. Géosciences Montpellier, Université de Montpellier, Montpellier, Languedoc-Roussillon, France  
pierre.camps@monpellier.fr
4. Statistics Department, Cal Poly State University, San Luis Obispo, CA 93407 USA  
mcarlton@calpoly.edu

**KEY WORDS:** Cenozoic lavas, paleomagnetism, geodynamo, transitional fields, reversal process

**Short Title:** Mantle control of the geodynamo

## SUMMARY

The degree to which the lower-most mantle influences behavior of the geodynamo has been debated over the past quarter century. Our analysis of a comprehensive set of 17 Cenozoic paleomagnetic transitional field records obtained from lavas in the Southern Hemisphere provides robust evidence of stable mantle control since the Pliocene. The records come from a region where—given a significantly weakened axial dipole—the magnetic field *today* would be largely controlled by the non-axial dipole (*NAD*) flux patch currently emanating from Earth's outer core beneath western Australia. The paleomagnetic recording sites from west to east include the south Indian Ocean, eastern

Australia, New Zealand, and French Polynesia. The analyzed records contain from 2 to 25 sequential transitional virtual geomagnetic poles (*VGP*s). Ten of the 17 records supply at least one *VGP* within a narrow longitudinal band 10°-wide between 60°S and the equator, centered along longitude 102.4°E. That is, transitional data from 59% of the Cenozoic recordings are found to reside in a region that encompasses a mere 2.8% of the *VGP* transitional area on Earth's surface. A robust Monte Carlo approach applied to this dataset, one that takes into account the number of transitional *VGP*s contained in each record, finds this result highly improbable ( $P$ -value = 0.0006). The present-day pattern of vertical flux at the core-mantle boundary shows an anomalously strong, thin Southern Hemisphere longitudinal band off the west coast of Australia that strikingly coincides with this unusual paleomagnetic finding. We conclude with a high degree of confidence that this band of flux has remained virtually unmoved for at least the past 3 Myr. Seemingly independent of the behavior of the axial dipole, our findings indicate it has dominated the magnetic field over an area of considerable size during attempts by the geodynamo to reverse polarity.

## 1. INTRODUCTION

The claim that the lowermost mantle exerts control over the morphology of the geomagnetic field first came to light from paleomagnetic findings showing preferred locations of transitional virtual geomagnetic poles (*VGP*s) (e.g. Laj *et al.* 1991; Hoffman 1992). Further support for the idea came from correlations of the paleomagnetic findings with aspects of the modern-day non-axial dipole (*NAD*) field and lower mantle seismic tomography (e.g. Constable 1992; Hoffman 1992). In particular, studies of Cenozoic lava sequences about the globe that recorded field behavior during times of transition

contain clusters, or groupings, of transitional *VGP*s at particular recurring localities (*e.g.* Hoffman 1992; Brown *et al.* 2000; Bogue *et al.* 2017), and most notably off the coast of western Australia (*e.g.* Chauvin *et al.* 1990; Roperch & Duncan 1990; Hoffman and Singer 2004; Hoffman *et al.* 2008) as well as the antipodal region (Mochizuki *et al.* 2011).

An alternative explanation of clustered transitional *VGP*s is that, rather than being due to extended stands by the vector field, the clusterings are artifacts of rapid-fire volcanic eruptions (*e.g.* Valet & Plenier 2008). That volcanic eruptions may occur episodically, sometimes at a rapid rate, is not debatable. Riisager *et al.* (2003) point out that one or both "types" of *VGP* clusters can be present in a single transitional field record. Nonetheless, there remains some question as to whether such paleomagnetic recurrences can ultimately prove long-term mantle control over the geodynamo. Here we shed light on the controversy with robust data that points strongly toward the affirmative.

## 2. THE AXIAL DIPOLE (*AD*) — NON-AXIAL DIPOLE (*NAD*) FIELD DICHOTOMY

The *NAD*-field is composed of the non-dipole field with the addition of the two equatorial dipole terms. (The *NAD* can also be referred to as the "*SAD*-field," "*S*" standing for the French *sans*; hence, unambiguously "the total field without the axial dipole term.") The dipole contribution to the entire geomagnetic field—specifically, the axial dipole (*AD*) term  $g_1^0$  determined from spherical harmonic analysis—is anomalously and uniquely strong not only at Earth's surface but also when calculated to the depth of the core-mantle boundary (*CMB*) (*e.g.* Courtillot *et al.* 1992). This finding alone suggests, if not a separation of the *AD*-field source from that responsible for the *NAD*-

field, no less than an enhanced generative efficiency of the former by the dynamo process. Analysis of the modern-day geomagnetic *NAD*-field (Fig. 1a) displays four particularly discernible vertical flux concentrations at Earth's surface (see Constable 2007a)—one each in North America, the south Atlantic, Siberia, and western Australia—that appear through the work of Jackson *et al.* (2000) to have remained stationary over the past 400 years (Fig. 1b).

Hoffman (1992) argues that core-mantle interactions are responsible for the primary features of the *NAD*-field flux pattern given Dziewonski & Woodhouse's 1987 seminal findings from normal mode seismic tomography of the lower mantle—specifically, the one-to-one correspondence seen between *NAD*-field maxima and those of fast *P*-wave velocity anomalies (Fig. 2, top left). Recent Stoneley mode predictions by Koelemeijer *et al.* (2017) of lowermost mantle heterogeneities (Fig. 2, top right) offer support for the state of these core-mantle boundary regions being anomalous, further suggesting that *NAD*-field morphology almost exclusively originates by way of fluid action at shallow depths within the outer core under the influence of varied boundary conditions at the base of the mantle. Also, several shear-wave tomographic models at 2800 km depth consistently show faster velocities at *NAD*-field maxima sites (Ritsema *et al.*, 2011); two such models are seen at the bottom of figure 2.

This shallow-core, mantle-influenced flux pattern, however, cannot be precisely the *NAD*; it will also contain a non-zero contribution from the  $g_1^0$  axial dipole term. Thus, in order to distinguish this part of the geomagnetic field appropriately we follow Hoffman & Singer (2008) and use the designation Shallow Core-generated (*SCOR*) field. Yet,

since the fraction of the observed *AD*-field arising from heterogeneous shallow core conditions is likely an insignificant fraction of the total axial dipole term and difficult to quantify, we will employ well-analyzed *NAD*-field constructions to closely approximate the *SCOR* in the study that follows.

During the one hundred years between 1900 and 2000 the primary *NAD*-field flux features remained spatially fixed while varying in strength at differing rates (see Hoffman & Singer 2004). For example, in the Southern Hemisphere the rate of change in strength of the flux patch beneath western Australia outpaced the patch in the South Atlantic. This differential in flux growth causes the rate of directional secular variation due to the *NAD*-field alone, here termed "*NAD-SV*," to be strongly site-dependent about the globe. Sites near a particular flux concentration will be mainly influenced by that particular patch; will be associated with *NAD*-field north (or south) virtual geomagnetic poles (*VGPs*) being strongly attracted to it; and will experience a low level of *NAD-SV*. Sites, say, equidistant between two flux patches will experience an influence by both; will likely be associated with *NAD*-field *VGPs* not in close proximity to either concentration; and, in general, will experience a high level of *NAD-SV*.

### 3. TRANSITIONAL FIELD RECORDS FROM THE LOW *NAD-SV* REGION

Figure 3 shows a contour map of angular change of *VGPs* associated with the *NAD*-field over the 20th Century (Hoffman & Singer 2008). Contoured color-coding, in increments of five degrees from 0°-to-5° (dark blue) to 40°-to-45° (deep red), shows the global pattern of this angular change. We classify regions of differing degrees of *NAD-SV* as follows: 0° to 15° of angular change as low; 15° to 30° as mid-range; and 30° to

45° as high. The darkest blue patches—representing minimal angular change—are seen in and around North America [1] and Siberia [2] and Australia [3], each near a location of strong sub-vertical flux. The Australian is the only patch of the four emanating upwardly directed flux, a distinction that may help to explain its extensive regional influence. Since the four *NAD*-field flux concentrations observed today appear to have had a dominating influence over the past 400 years (Fig. 1), the question we now explore is the time over which they may have persisted.

Assume as has been suggested that during those times when the *AD*-field was particularly weak, these flux features, especially the Australian patch, dominated the global field. Assume further that this particular patch of flux remained stably in place from the present over sufficient geologic time spanning several transitional field events. If so, then a measure of the time of its persistence may be gleaned from the paleomagnetic record of transitional field directions. Specifically, any site on Earth's surface within or in close proximity to the large low-*NAD-SV* (blue) region associated with the Australian flux patch would experience paleofield directions corresponding to either north or south *VGP*s (depending on sign) within or in close proximity to the flux patch, it being the primary magnetic field source.

We can test the above scenario by analyzing paleomagnetic transitional field records obtained from lava sequences at sites that today would experience a dominating effect from the Australian *NAD*-field flux patch given a significantly weakened *AD*-field. We chose the Australian patch for this analysis because of its widespread significance on 20th Century *NAD-SV* and the availability of numerous transitional field lava-based records from sites within its range of influence; we now focus our analysis on data from

sites found in and about the low *NAD-SV* centered near western Australia.

There are eight of these "blue-region" sites about the globe (Fig. 3) from which lava-based paleomagnetic transitional field records have been obtained. Of these, six are in the Southern Hemisphere—in the south Pacific, Australasia and the south Indian Ocean. The remaining two sites are in the Northern Hemisphere—in western North America and at the Hawaiian hotspot.

Virtual geomagnetic poles of each sign associated with all eight blue-region sites, calculated for the present-day *NAD*-field alone, and for the 400-year-averaged *NAD* from 1590 to 1990 (Jackson *et al.* 2000), are plotted in Fig. 4. For each site, regardless of being in the Northern or Southern Hemisphere, the two *VGP* determinations are found in close proximity to one another. This finding provides support for the contention that the *NAD* flux pattern is largely controlled by quasi-static conditions in the lower-most mantle at least during historical times. The question is: how far back into the geologic record can this apparent control be observed?

We exclude from our final analysis paleomagnetic data obtained from the two Northern Hemisphere sites (e.g. Bogue and Coe, 1984; Prévot *et al.* 1985; Leonhardt *et al.* 2009; Bogue *et al.* 2017). Although these sites experience some influence from the Australian flux patch, their associated *NAD*-fields are not dominated by it. Rather, their modern-day *NAD*-fields are far more affected by the flux concentration emanating from beneath North America, both sites being located along the periphery of the North American *NAD-SV* minimum (see Fig. 3).



#### 4. TRANSITIONAL *VGP*s AND ANALYSIS

The six Southern Hemisphere site localities have provided in total 17 lava-based records of transitional fields spanning the last ~40 Myr of the Cenozoic (Table 1). Figure 5 shows a compilation of 155 transitional *VGP*s—those which lie between 60°N and 60°S latitude—obtained from the 17 Southern Hemisphere blue-region site records. Sequences represented contain a minimum of two serially-recorded transitionally-magnetized lavas (Table 1). The choice of 60°—often chosen as the cutoff for transitional *VGP*s—is nonetheless arbitrary. There can be no universal cutoff for a transitional *VGP* since the relationship between directional rotation and pole migration is non-orthogonal (see Hoffman 1984a). Tectonic corrections were made for the four oldest records. A hotspot reference frame is used (see Appendix I for details), in which one implicitly assumes there to be no true polar wander (TPW) since ~37 Ma—which may or not be the case.

Since the dynamo is blind to the direction of magnetic flux lines, antipodal paleodirections are equivalent in so far as outer core fluid dynamics is concerned. That is, virtual poles may be treated as either north-*VGP*s or south-*VGP*s. This is the so-called "geomagnetic convention"—a procedure that has been shown to be helpful in recognizing aspects of the recorded dynamo reversal process (Hoffman 1984b; Prévot & Camps 1993; Love 1998; Hoffman & Mochizuki 2012)—which we now employ. We define north-*VGP*s and south-*VGP*s as follows: north-*VGP*s are those associated with paleodirections found in the paleomagnetic record (i.e. from the rocks). A south-*VGP* is the antipode to

that found in the rocks. That is to say, if, for example, two antipodal *VGP*s are calculated from paleodirections found in the same rock sequence, both are by definition north-*VGP*s.

Figure 6a is the geomagnetic-convention plot for the data shown in Fig. 5. Here each north-*VGP* in the Northern Hemisphere is displayed by its antipode in the Southern Hemisphere, that is, by its south-*VGP* equivalent. North-*VGP*s found in the Southern Hemisphere are unaffected. As can be seen, this procedure adds a significant number of *VGP*s to the Southern Hemisphere and, in particular, to the virtual pole grouping in the vicinity above the *NAD*-field flux concentration beneath Australia.

In contrast to past studies we employ an analytical procedure that does *not* tally the number of clusters present at a given location nor the total number of transitional *VGP*s contained within each cluster. Rather, our approach is to count the number of Southern Hemisphere blue-region *records* involved at a location, followed by an analysis of the distribution by means of a 10°-wide window of longitude. Figure 6b shows a plot of the number of records having one or more transitional *VGP*s (i.e. having latitude between 60°S and 0°) in each of the thirty-six 10°-wide longitudinal strips about the globe.

We focus attention now on the 10°-wide longitudinal strip we found to contain transitional virtual poles associated with the largest number of blue-region site records. This band, centered along longitude 102.4°E and highlighted in yellow in Fig. 6b, contains transitional *VGP*s from 11 of the 17 records. Although each longitudinal band comprises just 2.8% of global coverage between 60°S and the equator, more than half of

the available blue-region site datasets from the Southern Hemisphere are represented in this one narrow strip.

The significance of this finding depends largely on the number of transitional *VGP*s contained in each individual record in the analysis. While 2 of the records contain between 23 – 25 *VGP*s and 5 of the records contain between 13 – 15 *VGP*s, the remaining 10, 59% of the records, contain between just 2 – 7 transitional *VGP*s and 5 of these 10 "short" records contain at least one *VGP* within that particular 10°-wide band.

The Monte Carlo method was implemented in the R statistical software environment (R Core Team, 2013) to determine the empirical probability of obtaining such a distribution given the number of transitional *VGP*s in each of the analyzed records. The simulation's null hypothesis is that, for a record with  $n$  *VGP*s, the number that appear in any particular 10°-wide longitudinal band can be modeled by a binomial probability distribution with sample size  $n$  and success probability  $1/36$  (since  $10^\circ = 1/36$  of a circle). That is, the null hypothesis assumes that *VGP*s are equally likely to occur around the globe. Treating the 17 field records as independent observations, the Monte Carlo simulation recorded how many of those records would include at least one *VGP* in a specific 10° band under the assumed binomial model (see Appendix II for further details).

Of 100,000 Monte Carlo repetitions, only 60 resulted in ten or more of the 17 field records detecting transitional *VGP*s within any 10°-wide longitudinal band ( $P$ -value = 0.0006, or 0.06% "successes"), indicating statistically how highly unusual is this finding, regardless of the fact that the site distribution is not spatially uniform. Figure 7 shows the corresponding Monte Carlo frequency diagram, where the most probable outcome is just 3 - 4 such records.

It is tempting to conclude from this result that features of the magnetic flux pattern at the CMB—observed in the paleomagnetic record when the axial dipole had significantly weakened—have remained virtually stationary from the modern-day (Fig. 1) through much of the Cenozoic. However, on further examination one sees an asymmetry in the data—a bias by transitional records from the Plio-Pleistocene. Specifically, there are 11 such records, leaving just 6 older records spanning a significant time range from 9 Ma to nearly 40 Ma. We applied the Monte Carlo technique to each of these two separate groups of data. The 11 younger records (Fig. 8, top) strongly support the initial conclusion: of the 100,000 runs, only 258 (less than 0.3% “successes”) were found to lie in a 10° longitudinal band. Again, a highly unlikely result. The 6 older records (Fig. 8, bottom), however, do not satisfy such a conclusion: of the 100,000 runs 9,876 (nearly 10% “successes”) were found to lie in a 10° longitudinal band. Thus, we argue with confidence that the transitional data investigated here support stationarity of CMB primary flux features only through Plio-Pleistocene times—at least during the past 3 Myr.

## 5. EVIDENCE FROM PALEOINTENSITY DETERMINATIONS

The idea that geomagnetic field intensity may significantly drop during transitional events and that polarity reversals are accompanied by a decrease of 80% or 90% in dipole moment "is essentially undisputed" (Constable 2007b). If, however, primary *NAD-field* features along the CMB persist while the strength of the *AD-field* descends during a transitional event, then it is reasonable to suspect that sites at Earth's surface above one of these flux concentrations (see Fig. 1) would initially experience a far less significant reduction in field intensity than would the global average for that latitude. The claim of

persistence of the *NAD* can be tested given robust paleointensity determinations during transitional times at such a site. Camps *et al.* 2009 report such paleointensity values for Australian lavas at Liverpool Volcano, New South Wales, Australia, samples that record complex directional field behavior during the lower portion of the Eocene reversal. Their findings (Fig. 9; Appendix II) associated with 12 flows—5 reverse and 7 transitional, i.e. *VGP* latitudes  $>60^{\circ}\text{S}$  and  $<60^{\circ}\text{S}$ , respectively—show no obvious sign of any significant intensity decrease. Indeed, the determinations indicate that at least during this significant part of the reversal process the field strength, averaging  $\sim 36 \mu\text{T}$ , appear more closely aligned with what would be expected during non-transitional times of full polarity.

## 6. DISCUSSION

The modern-day vertical flux pattern at the core-mantle boundary (year 1990: Jackson *et al.* 2000) is shown in Fig. 10. Most noteworthy is the striking correspondence between the flux feature extending north-south from high to low latitudes off the west coast of Australia, and the  $10^{\circ}$ -wide longitudinal strip of Cenozoic transitional *VGP* seen in Fig. 6a. This flux feature is also clearly observed from measurements of more recent magnetic survey satellite orbits (e.g. Le Mouél *et al.* 2010). We argue that this surprisingly strong correspondence between Cenozoic transitional fields and the pattern of radial flux presently leaving the outer core provides to date the most significant evidence of tight, long-term mantle control of transitional field morphologies.

Hoffman & Singer (2004) have shown (see their fig. 3) that throughout the 20th Century, *NAD*-field *VGP*s associated with sites throughout Australasia correlate well with the CMB flux feature off the west coast of Australia. Indeed, the distribution of

modern-day *NAD*-field *VGP*s from these sites is astonishingly similar to the narrow longitudinal strip of dense transitional *VGP*s through much of the Cenozoic.

Expanding on the modern-day *NAD*-field *VGP* analysis to sites spanning the globe, the correlation strengthens: Figure 11 shows the modern-day *NAD*-field *VGP* pattern associated with 1,368 sites about the globe between latitudes 45°N and 45°S where it is seen that the majority of virtual poles are found along a well-focused, sub-longitudinal band passing along the west coast of Australia and continuing northward. This finding supplies further evidence that the Southern Hemisphere flux feature observed today at the CMB (Fig. 10) has been a major contributor to the global *NAD*-field over a significant span of geologic time.

These findings also suggest that the observation of "preferred" *VGP* pathways (Laj *et al.* 1991) is a phenomenon not altogether caused by longitudinal migration of mobile flux patches at the top of the core, as was first posited by Gubbins & Coe (1993). Rather, the similarity in the pattern of Cenozoic transitional *VGP*s (Fig. 4), and modern-day *NAD*-field *VGP*s associated with the same sites (Fig. 3), suggests that such field behavior during geomagnetic reversals and events is a consequence of competition among fixed magnetic sources. That is, these pathways may be due to a simple vector addition of the *NAD*-rich *SCOR*-field from sources near the core surface, and the *AD*-field from sources mainly generated elsewhere, presumably at further depth. Moreover, the fact that 7 of the 17 blue-region datasets (Table 1) are not records of polarity transitions, but rather geomagnetic excursions and events, provides additional evidence that the same dynamo process is at work regardless of whether or not a triggered event culminates in a change of polarity. Hence, such incomplete events may best be considered aborted reversals

(e.g. Hoffman 1981; Valet *et al.* 2008).

In summary, our findings strongly suggest that the *NAD*-field is largely a consequence of mantle-held flux anomalies at the core surface, and rather than vanishing with the axial dipole, appears to dominate the global transitional field during reversal attempts. If so, then the suggestion by Hoffman & Singer (2008) that the primary source(s) of the *AD*-field are in some manner separated from those responsible for the *NAD* (see also Constable, 1992; Hoffman, 1992; Camps and Prévot, 1996) becomes an appropriate issue to explore:

Terms arrived at through spherical harmonic analyses of Earth's magnetic field can be separated into two distinct categories, the so-called dynamo families (Roberts & Stix 1972). The Primary Dynamo Family ( $E_A$ ) is associated with components of the field that are antisymmetric about the equator, and the Secondary Dynamo Family ( $E_S$ ) is associated with components of the field that are symmetric about the equator. McFadden *et al.* (1991) showed that full-polarity paleomagnetic dispersion data recorded about the globe could be analyzed so as to quantify the relative importance to paleosecular variation (PSV) by each of the two families. What the authors found was that the variability in the  $E_S/E_A$  ratio positively correlated with reversal frequency since the Cretaceous Long Normal period. This claim has been strongly challenged by Biggin *et al.* (2008) and quite recently Doubrovine *et al.* (2019). However controversial, when considered along with the results of this study, we argue that McFadden *et al.*'s suggestion that the degree of interaction between members of the two dynamo families is key to understanding the triggering process for dynamo reversal is worthy of further investigation:

Theory has it that the two families can act separately only under certain idealized conditions. However, these conditions for non-interaction are hypothetical and apparently unrealistic, e.g. the mean velocity field of the core fluid must be symmetric, and therefore, non-turbulent (see Jacob 1994). Hence, although the paleomagnetic dynamo family-related dispersion data are intriguing, it is difficult to explain how members of the  $E_S$  family can trigger an attempted field reversal—unless the source of the bulk strength of each family is physically distinct.

By definition, the *NAD*-field contains the entire membership of the Secondary Dynamo Family along with all Primary Family members apart from its most important term, the axial dipole. How then the morphology of fluid flow at depth containing axial dipole flux adjusts to changing thermally-induced energetic conditions may determine the degree of interaction with shallow core flux. Therefore, if the *NAD*-field is in some manner the product of flux manipulation in the shallow core by the lowermost mantle, and as suggested by Hoffman & Mochizuki (2012), reverses polarity at a different time from that of the axial dipole, then it follows that times of strong interaction between shallow core flux and deeper-sourced *AD*-flux may be the initial stage of an attempt by the dynamo to reverse polarity.

## 7. CONCLUSION

For the case of the Southern Hemisphere we have shown that both the modern-day non-axial dipole (*NAD*) field pattern, and paleomagnetic transitional field data obtained from sites spanning a sizable region of the hemisphere, are linked to the most significant vertical flux anomaly emanating today from the fluid core. This anomaly, and hence the



associated *NAD*-field pattern, we argue, owe their existence to some form of flux manipulation brought about by heterogeneities in the shallow-most part of the core. The presented data indicate that this flux feature at the CMB has remained stationary for at least the past 3 Myr, and that it has regionally dominated the remaining field when the axial dipole has significantly weakened during attempts by the dynamo to reverse polarity. Available paleointensity determinations during a time of transitional field behavior experienced at an appropriate site are consistent with this claim.

Since the *NAD*-field is comprised by the entire membership of the "Secondary" (symmetric field) dynamo family, while excluding the most important component of the "Primary" (antisymmetric field) dynamo family—the axial dipole—this paleomagnetic study provides further evidence consistent with the view that the source of the *NAD* is independent from that which generates the bulk of axial dipole flux. If so, we suggest that such a two-tiered system may be a key element in the complete understanding of dynamo reversal initiation.

#### REFERENCES:

- Biggin, A.J., van Hinsbergen, D.J.J., Langereis, C.G., Straathof, G.B. & Deenen, M.H.L., 2009. Geomagnetic Secular variation in the Cretaceous Normal Superchron and in the Jurassic. *Physics Earth Planet. Int.*, **169**, pp.3. doi:10.1016/j.pepi.2008.07.004.hal-00532159.
- Bogue, S. W., & Coe, R.S., 1984. Transitional paleointensities from Kauai, Hawaii, and geomagnetic reversal models, *J. Geophys. Res.*, **89**, 10341-10354.
- Bogue, S.W., Glen, J.M.G. & Jarboe, N.A., 2017. Directional change during a Miocene R-N geomagnetic polarity reversal recorded by mafic lava flows, Sheep Creek Range, north central Nevada, USA, *Geochem. Geophys. Geosyst.*, **18**, 3470–3488,

doi:10.1002/2017GC007049.

- Brown, L., Singer, B.S., Pickens, J., & Jicha, B., 2004. Transitional magnetic field geometry during the Matuyama-Brunhes reversal: paleomagnetic and geochronologic data from the Tatara-San Pedro volcanic complex, Chilean Andes. *J. Geophys. Res.*, **109**, doi:10.1029/2004JB003007.
- Camps, P., Henry, B., Prévot, M. & Faynot, L., 2001. Geomagnetic paleosecular variation recorded in Plio-Pleistocene volcanic rocks from Possession Island (Crozet Archipelago, southern Indian Ocean), *J. Geophys. Res.*, **106** B2, 1961-1971.
- Camps, P. & Prévot, M., 1996. A Statistical Model of the Fluctuations in the Geomagnetic Field from Paleosecular Variation to Reversal, *Science*, **273**, 776-779.
- Carvallo, C., Camps, P., Ruffet, G., Henry, B. & Poidras, T., 2003. Mono Lake or Laschamp geomagnetic event recorded from lava flows in Amsterdam Island (southeastern Indian Ocean), *Geophys. J. Int.*, **154**, 767-782.
- Cassidy, J., 2006. Geomagnetic excursion captured by multiple volcanoes in a monogenetic field, *Geophys. Res. Lett.*, **33**, L21310, doi:10.1029/2006GL027284.
- Chauvin, A., Roperch, P. & Duncan, R.A., 1990. Records of geomagnetic reversals from volcanic islands of French Polynesia, 2, paleomagnetic study of a flow sequence (1.2–0.6 Ma) from the island of Tahiti and discussion of reversal models. *J. Geophys. Res.*, **95**, 2727–2752.
- Constable, C., 1992. Link between geomagnetic reversal paths and secular variation of the field over the last 5 Myr., *Nature.*, **358**, 230–233.
- Constable, C.G., 2007a. in *Encyclopedia of Geomagnetism and Paleomagnetism*, edited by D. G. Gubbins & E. Herrero-Bervera, pp. 701–704, Springer, Dordrecht, Netherlands, doi:10.1007/978-1-4020-4423-6\_22.
- Constable, C.G., 2007b. in *Encyclopedia of Geomagnetism and Paleomagnetism*, edited by D. G. Gubbins & E. Herrero-Bervera, pp. 159–161, Springer, Dordrecht, Netherlands, doi:10.1007/978-1-4020-4423-6\_22.
- Constable, C.G. & Parker, R.L., 1988. Statistics of the geomagnetic secular variation for the past 5 Ma. *J. Geophys. Res.*, **93**, 11569-11582.
- Courtillot, V., Valet, J.-P., Hulot, G. & Le Mouél, J.-L., 1992. The Earth's magnetic field: Which geometry?, *EOS*, **73**, 337-342, doi:10.1029/91EO00260.

- Cox, A. & Hart, R.B., 2009. *Plate Tectonics: How It Works*, Wiley-Blackwell, ISBN: 978-1-444-31421-2, pp. 416.
- Dobrovine, P.V., Veikkolainen, T., Pesonen, L.J., Piispa, E., Ots, S., Smirnov, A.V., Kulakov, E.V. & Biggin, A.J. 2019. Latitude dependence of geomagnetic paleosecular variation and its relation to the frequency of magnetic reversals: Observations from the Cretaceous and Jurassic, *Geochem. Geophys Geosys*, doi.org/10.1029/2018GC007863.
- Dziewonski, A. & Woodhouse, J., 1987. Global images of the Earth's interior, *Science*, **236**, 37-48.
- Gubbins, D.R. & Coe, R.S., 1993. Longitudinally Confined Geomagnetic Reversal Paths from Non-Dipolar Transition Fields, *Nature*, **362**, 51-53.
- Hoffman, K.A., 1981. Palaeomagnetic excursions, aborted reversals and transitional fields, *Nature*, **294**, 67-69, doi:10.1038/294067a0.
- Hoffman, K. A., 1984a. A Method for the Display and Analysis of Transitional Paleomagnetic Data, *Jour. Geophys. Res.*, **89**, 6285-6292.
- Hoffman, K.A., 1984b. Geomagnetic reversals, *Nature*, **309**, 90-91.
- Hoffman, K.A., 1986. Transitional field behavior from southern hemisphere lavas: evidence for two-stage reversals of the geodynamo. *Nature*, **320**, 228-232, doi:10.1038/320228a0.
- Hoffman, K.A., 1992. Dipolar reversal states of the geomagnetic field and core–mantle dynamics. *Nature*, **359**, 789–794., doi:10.1038/359789a0.
- Hoffman, K.A. & Mochizuki, N., 2012. *Geophys. Res. Lett.*, **39**, L06303, doi:10.1029/2011GL050830.
- Hoffman, K.A. & Singer, B.S., 2004. Regionally recurrent paleomagnetic transition fields and mantle processes. In: Channell, J.E.T., Kent, D.V., Lowrie & W., Meert, JgG., (Eds.), *Timescales of the Paleomagnetic Field*. AGU, Geophysical Monograph, vol. 145. American Geophysical Union, Washington, DC, pp. 233–243, doi:10.1029/145GM17.
- Hoffman, K.A. & Singer, B.S., 2008. *Science*, **B**, 1800, doi:10.1126/science.1159777.
- Hoffman, K.A., Singer, B.S., Camps, P., Hansen, L.N., Johnson, K.A. Clipperton, S & Carvallo, C., 2008. Stability of mantle control over dynamo flux since the mid-

- Cenozoic, *Phys. Earth Planet. Int.*, **169**, 20-27, doi:10.1016/j.pepi.2008.07.012.
- Jackson, A., Jonkers, A. & Walker, M., 2000. Four centuries of geomagnetic secular variation from historical records. *Phil. Trans. R. Soc. Lond.*, **358**, 957–990.
- Jacobs, J.A., 1994. *Reversals of the Earth's Magnetic Field*, 2nd edition, Cambridge University Press, Cambridge pp. 346.
- Koelemeijer, P., Deuss, A. & Ritsema, J., 2017. Density structure of Earth's lowermost mantle from Stoneley mode splitting observations, *Nature Communications*, **8**, 15241, doi:10.1038/ncomms15241.
- Kustowski B., Ekström, G. & Dziewonski A.M., 2008. The anisotropic shear-wave velocity structure of the Earth's mantle, *J. geophys. Res.*, **1390**, doi:10.1029/2007JB005169.
- Laj, C., Mazaud, A., Weeks, R., Fuller, M. & Herrero-Bervera, E., 1991. Geomagnetic reversal paths. *Nature*, **351**, 447, doi:10.1038/351447a0.
- Le Mouél, J.L., Shebalin, P. & Khokhlov, A., 2010. Earth magnetic field modeling from Oersted and Champ data, *Ear. Planet. Space*, **62**, 277-286.
- Leonhardt, R., McWilliams, M., Heider, F. & Soffel, H.C., 2009. The Gilsá excursion and the Matuyama/Brunhes transition recorded in  $^{40}\text{Ar}/^{39}\text{Ar}$  dated lavas from Lanai and Maui, Hawaiian Islands, *Geophys. J. Int.*, **179**, 43-58, doi.org/10.1111/j.1365-246X.2009.04264.x
- Love, J.J., 1998. Palcomagnetic volcanic data and geometric regularity of reversals and excursions, *J. Geophys. Res.*, **103**, 12,435-12,452.
- McFadden, P.L., Merrill, R.T., McElhinny, M.W. & Lee, S., 1991. Reversals of the Earth's magnetic field and temporal variations of the dynamo families, *J. Geophys. Res.*, **96**, 3923-3933.
- Mochizuki, N., Oda, H., Ishizuka, O., Yamazaki, T. & Tsunakawa, H., 2011. Paleointensity variation across the Matuyama-Brunhes polarity transition: Observations from lavas at Punaruu Valley, Tahiti, *J. Geophys. Res.*, **116**, B06103 doi:10.1029/2010JB008093.
- Müller, R.D., Gaina, C., Tikku, A., Mihut, D., Cande, S.C. & Stock, J.M., 2000. Mesozoic/Cenozoic tectonic events around Australia, In: *The History and Dynamics of Global Plate Motions*, Geophysical Monograph 121, 161-188,

doi:10.1029/GM121p0161.

Plénier, G., Camps, P., Henry, B. & Nicolaysen, K., 2002. Palaeomagnetic study of Oligocene (24-30 Ma) lava flows from the Kerguelen Archipelago (southern Indian Ocean): directional analysis and magnetostratigraphy, *Phys. Earth Planet. Int.*, **133**, 127-146.

Prévot, M. & Camps, P., 1993. *Nature*, **366**, 53-57, doi:10.1038/366053a0.

Prévot, M., Mankinen, E.-A., Grommé, C.S. & Coe, R.S., 1985. How the geomagnetic field vector reverses polarity. *Nature*, **316**, 230-234.

R Core Team (2013). R: A language and environment for statistical computing. R Foundation for Statistical Computing, Vienna, Austria. URL <http://www.R-project.org/>.

Ritsema, J., Deuss, A., van Heijst, H. J. & Woodhouse, J. H., 2011. S40RTS: a degree-40 shear-velocity model for the mantle from new Rayleigh wave dispersion, teleseismic traveltime and normal-mode splitting function measurements, *Geophys. J. Int.*, **184**, 1223–1236, doi:10.1111/j.1365-246X.2010.04884.x

Riisager, J., Riisager, P. & Pedersen, A.K., 2003. The C27n-C26r geomagnetic polarity reversal recorded in the west Greenland flood basalt province: How complex is the transitional field?, *J. Geophys. Res.*, **108**, doi:10.1029/2002JB002124.

Roberts, P.H. & Stix, M., 1972.  $\alpha$ -effect dynamos, by the Bullard-Gellman formalism, *Astron. & Astrophys.*, **18**, 453-466.

Roperch, P. & Duncan, R.A., 1990. Records of geomagnetic reversals from volcanic islands of French Polynesia: 1. Paleomagnetic study of a polarity transition in a lava sequence from the Island of Huahine, *J. Geophys. Res.*, **95**, 2713–2726, doi:10.1029/JB095iB03p02713.

Schettino, A. & Scotese, C.R., 2005. Apparent polar wander paths for the major continents (200 Ma to the present day): a palaeomagnetic reference frame for global plate tectonic reconstructions, *Geophys. J. Int.*, **163**, 727–759, <https://doi.org/10.1111/j.1365-246X.2005.02638.x>

Singer, B.S., 2014. A Quaternary geomagnetic instability time scale, *Quaternary Geochronology*, **21**, 29-52.

Tetley, M.G., Williams, S.E., Gurnis, M., Flament, N., & Müller, R.D., 2019.

Constraining absolute plate motions since the Triassic, *J. Geophys. Res.*, **124**, doi:10.1029/2019JB017442.

Valet, J.-P. & Plenier, G., 2008. Simulations of a time-varying non-dipole field during geomagnetic reversals and excursions, *Phys. Earth planet. Int.*, **169**, 178-193.

Valet, J.-P., Plenier, G. & Herrero-Bervera, E., 2008. Geomagnetic excursions reflect an aborted polarity state, *Earth Planet. Sci. Lett.*, **274**, 472-478.

Yamamoto, Y., Ishizuka, O., Sudo, M. & Uto, K., 2007.  $^{40}\text{Ar}/^{39}\text{Ar}$  ages and paleomagnetism of transitionally magnetized volcanic rocks in the Society Islands, French Polynesia: Raiatea excursion in the upper-Gauss Chron, *Geophys. J. Int.*, **169**, 41-59, doi: 10.1111/j.1365-246X.2006.03277.

Acknowledgments: We thank Pavel Doubrovine and Roman Leonhardt for insightful reviews of the original manuscript. The first author (KAH) wishes to thank the National Science Foundation for its continued support through grant #EAR1015360.

## APPENDICES

### APPENDIX I. Plate-tectonic reconstruction method employed

The finite rotation poles used to transfer the virtual geomagnetic poles into the Earth's spin axis reference frame are marked in bold characters in the following table. They are calculated from Schettino & Scotese (2005) and the OptAPM1-M16 reconstruction model of Tetley *et al.* (2019) by means of a global circuit through the central Africa.

To achieve increased accuracy, we interpolated within these models the Euler poles at the age of the volcanic sequences considered in the present study. For this purpose, we calculated the stage pole as explained in Cox & Hart (Chap. 7, 2009) assuming that the rate of motion and the direction of motion do not change within the time interval yielded in the plate motion models. We combined the successive rotations within the global circuit through central Africa into a single rotation by means of matrix multiplications following the properties of the nonabelian group SO(3) (e.g., Cox & Hart 2009).

Plate ID / fixed Plate ID	Euler Pole		
	Lat(°)	Long(°)	Angle(°)
<i>Kaputar : Time 18 Ma</i>			
801/802	-15.10	213.17	10.74
802/701	10.36	311.90	2.49
701/001	59.15	-64.44	-4.61
801/001	-32.92	211.74	11.63
<i>Quamby Fall : Time 26.5 Ma</i>			
801/802	-14.47	213.14	16.13
802/701	11.55	311.77	4.10
701/001	55.28	-59.84	-6.81
801/001	-30.46	211.03	17.39
<i>Liverpool : Time 37 Ma</i>			

801/802	-15,45	211.34	22.17
802/701	11.76	313.75	6.33
701/001	49.81	-54.16	-9.21
	-29.23	208.83	23.86
<i>Kerguelen : Time 27 Ma</i>			
802/701	11.60	311.76	4.20
701/001	55.04	-59.64	-6.95
802/001	-82.44	22.55	4.92

Where the plate IDs are :

001 : Present Day Atlantic/Indian Hotspots  
 701 : African Craton  
 801 : Australia  
 802 : Antarctica and East Antarctica.

---

## APPENDIX II Details of the employed Monte Carlo method

Take the 11 younger flows, for example. Each has a different number of transitional *VGP*s. For each loop of the simulation, the following was done:

1. Eleven binomial random variables were generated. Each one has an "n" equal to the number of *VGP*s in the record; e.g. X1 has n=14, X2 has n=6, and so on. All 10 of them use  $p=1/36$ , the probability of a *VGP* falling into the particular 10-degree window of interest.
2. The number of binomial random variables  $\geq 1$  were counted. So, randomly, and with the number of observed *VGP*s in each record, how many records out of 11 would we expect to show at least one *VGP* in the 10-degree window? That count, anything from 0 through 11, is graphed at the top of figure 8.



3. Since 7 of the 11 records had at least one *VGP* in the window of interest, the (empirical) *P*-value is the chance of 7 or more binomial random variables of being positive. (For this case, that value turns out to be super-small.)

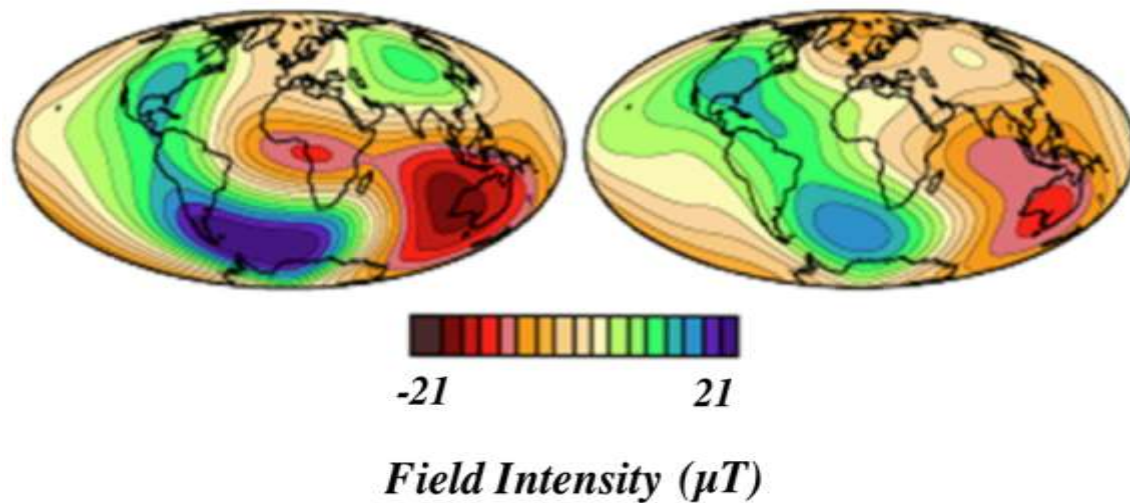


Fig. 1: Vertical component of the non-axial dipole (*NAD*) field at Earth's surface: (left) Year 2000 (Constable 2007); (right) 400-year average from 1590 to 1990 (Jackson *et al.* 2000).

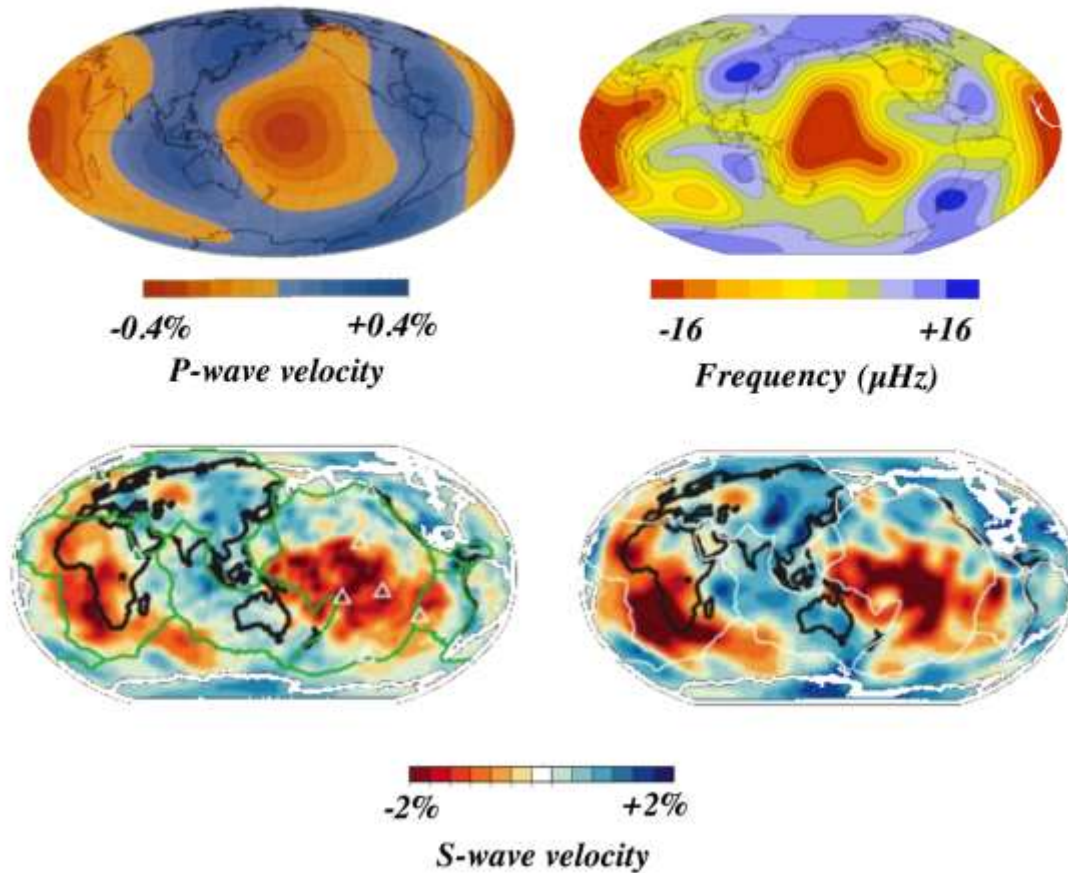


Fig. 2: (top left) Normal mode analysis of  $P$ -wave velocity anomalies at a depth of 2300 km, blue and orange regions denoting fast and slow velocity anomalies, respectively (from Dziewonski & Woodhouse, 1987). (top right) Predicted Stoneley mode splitting of  ${}_2S_{16}$  at 2800 km depth for shear-and-compressional-wave velocity model SP12RTS (from Koelemeijer et al., 2017). Note in both cases the strong correspondence with primary  $NAD$ -field features in figure 1. (The same features, however, are not clearly predicted for Stoneley mode  ${}_3S_{16}$ .) (bottom) Shear wave velocity anomalies for models S40RTS (Ritsema et al., 2011) and S362ANI (Kustowski et al., 2008). Again, fast velocity anomalies (in blue) are associated with regions of  $NAD$ -field maxima.

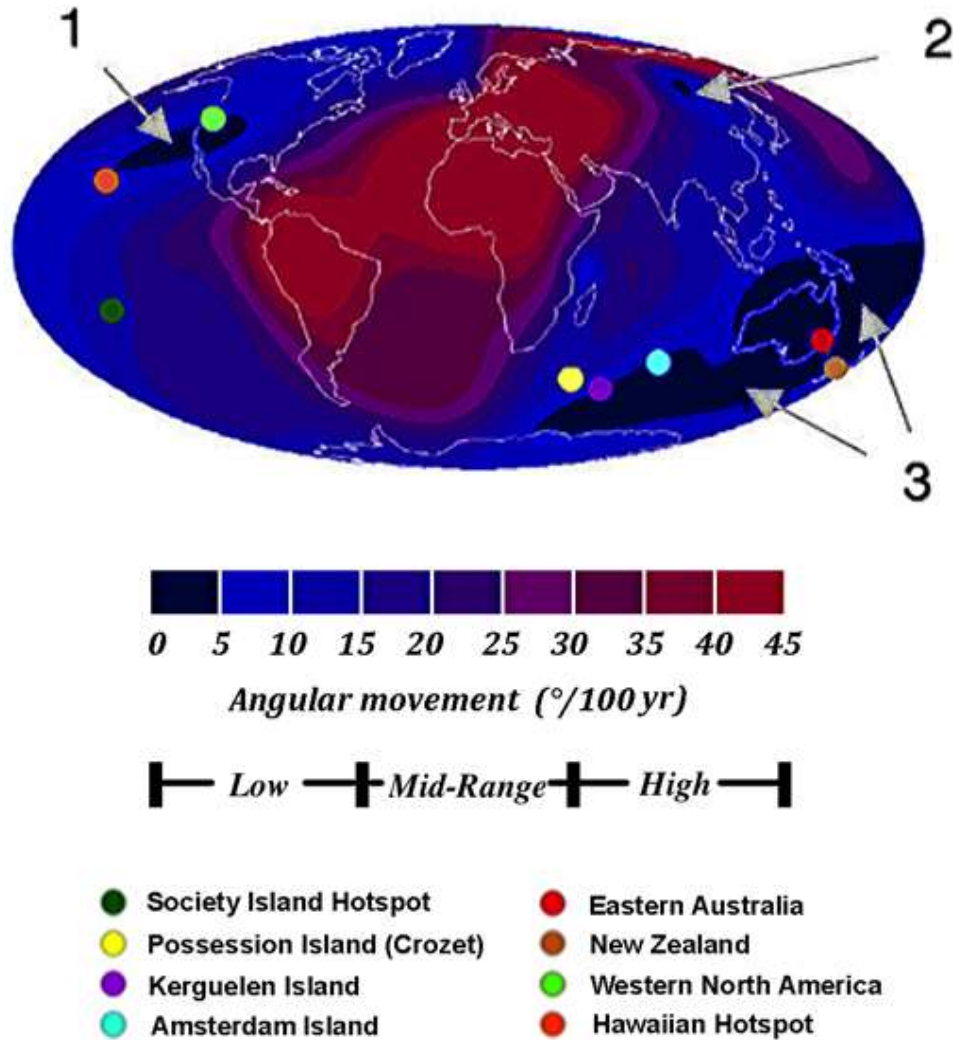


Fig. 3: Contour map of angular change of VGP associated with the NAD-field over the 20th Century. Deeper shades of blue and red represent lower and higher degrees, respectively, of this secular change (after Hoffman & Singer 2008). Minima (deepest shade of blue) are found along the west coast of North America (1); in Siberia (2); and throughout a sizeable region centered in Australasia (3). Superposed are blue-region sites ( $<15^{\circ}$  of movement) from which lava-based transitional field records have been obtained (color-coded as indicated).

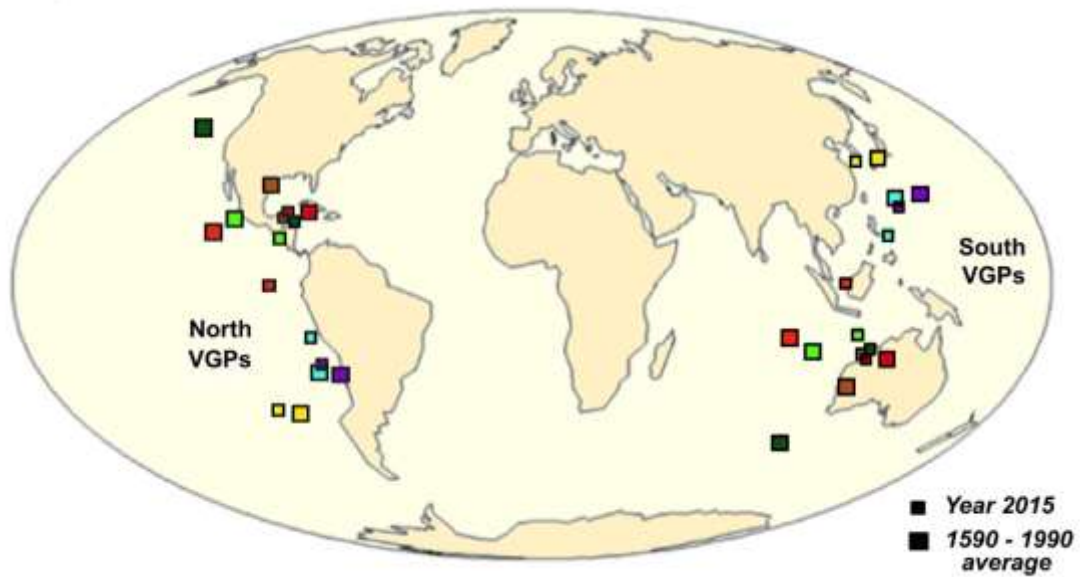


Fig. 4: Calculated *VGPs* associated with the present-day *NAD*-field and the average historic *NAD*-field for the sites shown in Fig. 3. Both north *VGPs* and south *VGPs* are displayed as indicated and color-coded corresponding to the site.

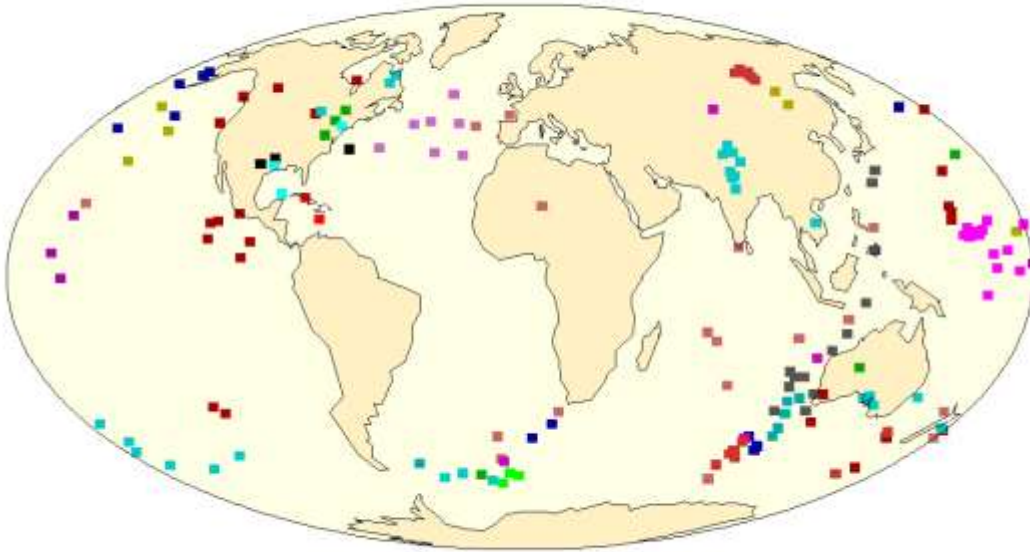


Fig 5: All transitional *VGPs* from 17 paleomagnetic records obtained from sites that roughly surround Australasia (see Table 1).

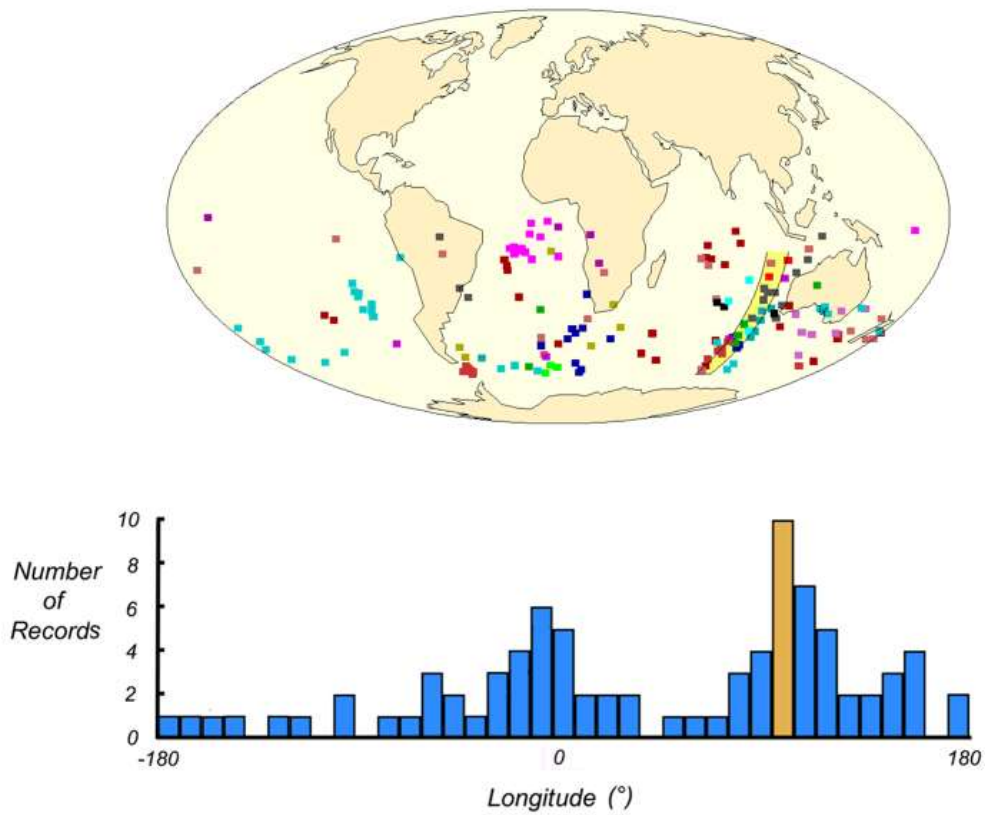


Fig 6: (top) All transitional VGP's contained in 17 paleomagnetic records from sites shown in Fig. 3 employing the geomagnetic convention. Each is uniquely color-coded (see Table 1). (bottom) Graph of the number of records having at least one VGP for each 10°-wide band of longitude about the earth. The most populated band centered on longitude 102.4°E is highlighted.



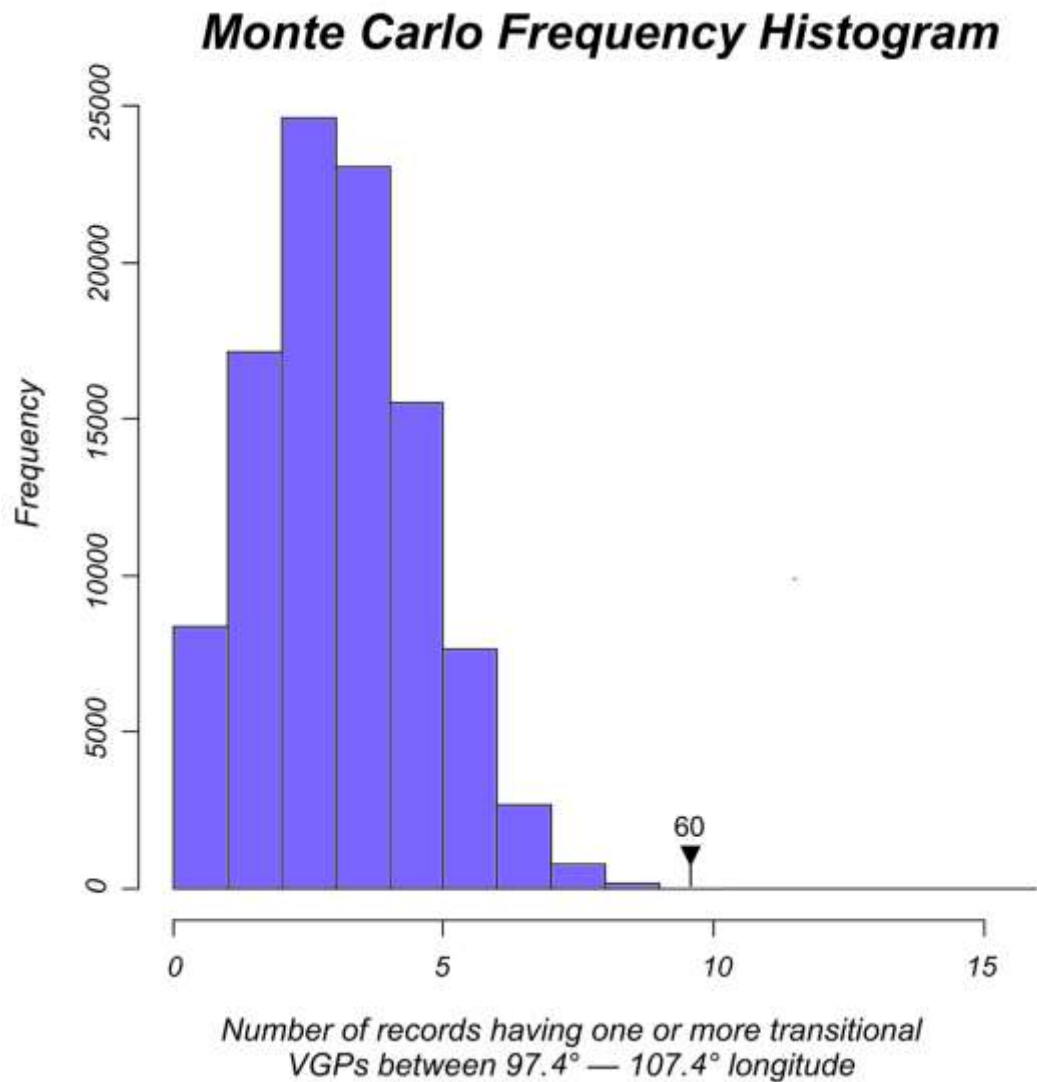


Fig. 7: Monte Carlo results: Given the number of transitional VGPs displayed for each of the 17 records listed in Table I, the frequency of occurrence is shown as a function of the number of records having at least one virtual pole within a 10°-wide longitudinal band (100,000 runs). For 10 records only 60 Monte Carlo runs give such a result ( $P$ -value = 0.0006).



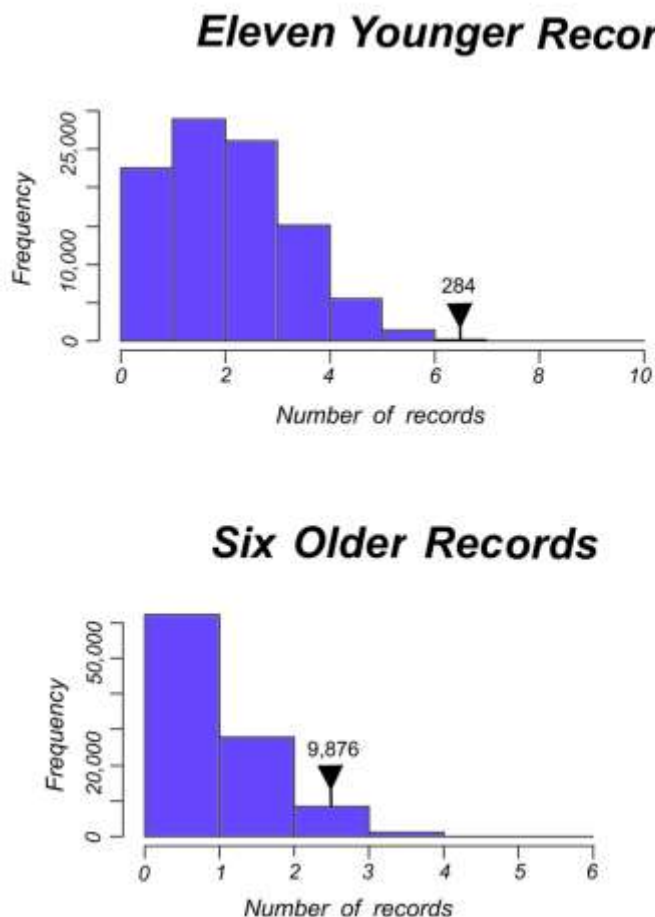


Fig. 8: (*top*) Frequency of occurrence as a function of the number of younger records (Pliocene — Quaternary) having at least one virtual pole within a  $10^\circ$ -wide longitudinal band (100,000 runs). Note: 7 of these 11 records contain such a VGP, while the most probable number is two. Only 258 Monte Carlo runs give such a result ( $P$ -value = 0.00258). (*bottom*) Frequency of occurrence as a function of the number of older records (Eocene — Miocene) having at least one virtual pole within a  $10^\circ$ -wide longitudinal band (100,000 runs). Note: 3 of these 6 records contain such a VGP, while the most probable number is one. 9,876 Monte Carlo runs give such a result ( $P$ -value = 0.09876).

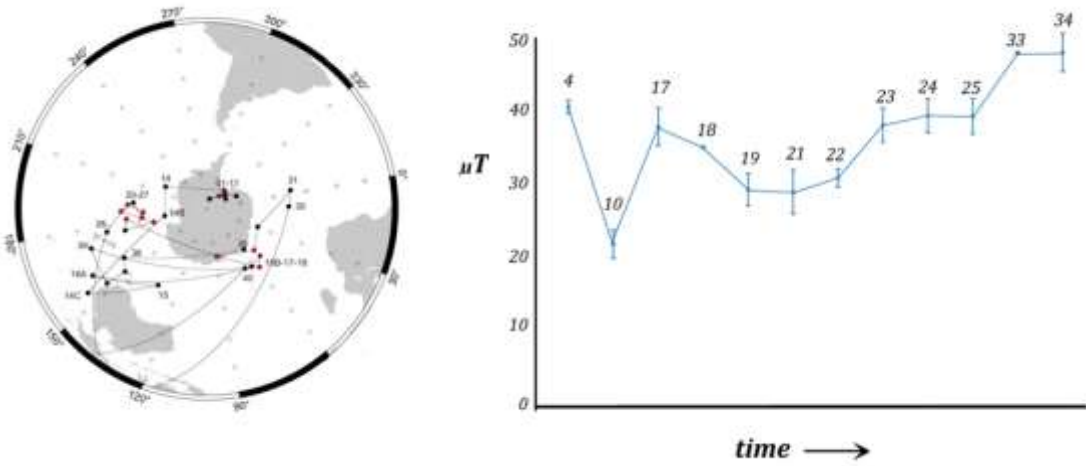


Fig. 9: Southern Hemisphere VGPs during the lower portion of the Liverpool reversal (at left) along with determinations of paleointensity in chronological order (at right). Flow numbers are shown. Note the near complete lack of expected, weak transitional field strengths at the Liverpool site. (data from Camps *et al.* 2009)

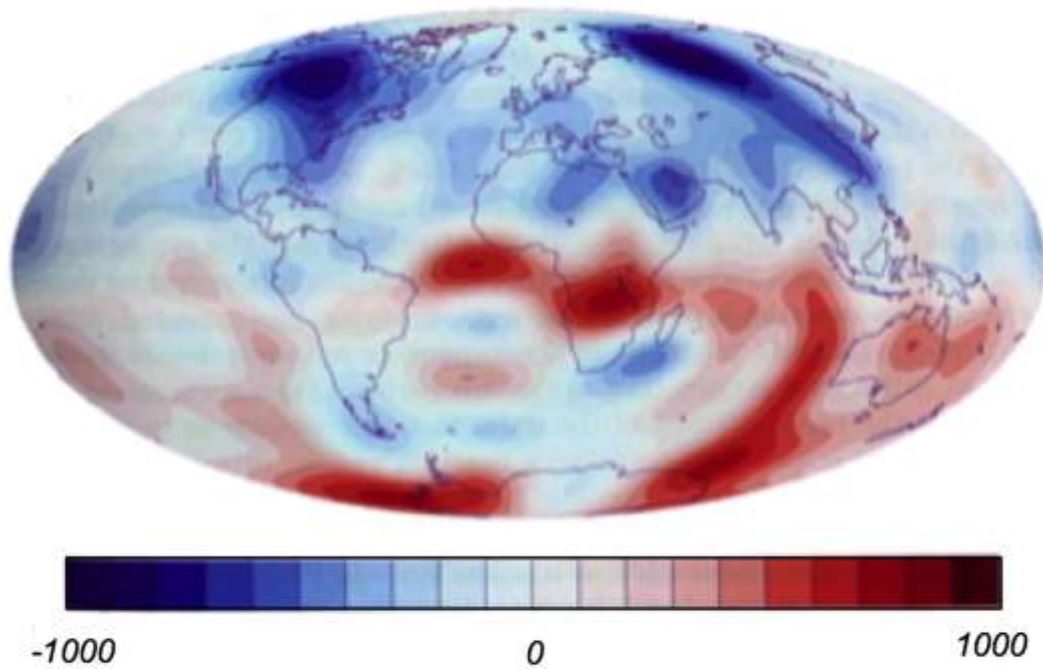
















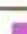


Fig. 10: The vertical geomagnetic field at the core-mantle boundary for the year 1990 (Jackson *et al.* 2000). Deepness in shade correlates with field strength. Red and blue denote upward and downward directed field lines, respectively. Contour interval is  $100\mu\text{T}$ .

Note the correspondence between the most significant Southern Hemisphere flux feature west of Australia with the most highly-populated longitudinal band of transitional VGP's shown in Fig. 6.



Fig. 11: The pattern of modern-day *NAD*-field south *VGP*s associated with 1,368 sites between 45°N and 45°S latitudes about the globe.

**Table 1: Transitional field records from low *NAD-SV* (blue-region) sites**

Lava Location	Eruption Site	Event	Age	Color	a / b*	Refs
New Zealand; North Island	Present Day Site Location	Mono Lake Excursion	~32 ka		0/13 (0%)	Cassidy (2006)
Tahiti	Society Island Hotspot	Los Tilos Event	~590 ka		6/13 (46%)	Hoffman & Singer (2004) Singer (2014)
*	"	Matuyama-Brunhes R-N	~776 ka		2/6 (33%)	Chauvin et al. (1990)
*	"	Matuyama-Brunhes R-N	~776 ka		3/6 (50%)	Mochizuki et al. (2011)
"	"	Jaramillo-Matuyama N-R	~1.00 Ma		1/23 (4%)	Chauvin et al. (1990)
"	"	Punaruu Event	~1.12 Ma		3/13 (23%)	Chauvin et al. (1990) Singer (2014)
Huahine	"	Pliocene event	~2.9 Ma		2/17 (12%)**	Roperch & Duncan (1990)
Raiatea	"	Raiatea Excursion	~2.77 Ma		0/6 (0%)	Yamamoto et al. (2007)
Taha'a	"	Mammoth R-N (?)	~3.20 Ma		0/4 (0%)	Yamamoto et al. (2007)
Amsterdam Island	Present Day Site Location	Brunhes Excursion	Late Brunhes		1/2 (50%)	Carvallo et al. (2003)
Possession (Crozet) Island	"	Normal Polarity Excursion	Pliocene		0/3 (0%)	Camps et al. (2001)
Kerguelen Island	Plate Tectonically-Corrected Oligocene Site Location***	Oligocene N-R	~28 Ma		1/4 (25%)	Plerier et al. (2002)
Queensland, Australia	Plate Tectonically-Corrected Oligocene Site Location***	Quamby Falls R-N	~26.5 Ma		5/15 (33%)	Hoffman et al. (2008)
New South Wales, Australia	Plate Tectonically-Corrected Eocene Site Location***	Liverpool R-N	~37 Ma		0/28 (0%)	Hoffman (1986)
New South Wales, Australia	Plate Tectonically-Corrected Miocene Site Location***	Mt. Kaputar Excursion	~18 Ma		0/7 (0%)	Hoffman (1986)
New Zealand; South Island	Present Day Site Location	Akaroa N-R	9.51 Ma		1/3 (33%)	Hoffman (1986)
*	"	Akaroa R-N	9.67 Ma		0/3 (0%)	Hoffman (1986)

\* a / b # Southern Hemisphere transitional VGPs between 97.4°–107.4° / # transitional VGPs

\*\* Directional groups constructed by Roperch & Duncan (1990) from 66 transitional VGPs, 8 (12%) of which lie between 97.4°–107.4°.

\*\*\* See Appendix I